ARMY RESEARCH LABORATORY

Progress in Materials Synthesis and Processing of Barium Titanium Oxide ($BaTiO_3$) and Barium Strontium Titanium Oxide ($BaTiSrO_3$) Films for Uncooled Infrared (IR) Detector Applications

by Wendy L. Sarney, Kimberley A. Olver, John W. Little
Frank E. Livingston, Krisztian Niesz, and Daniel E. Morse

ARL-TR-5853 **December 2011**

NOTICES

Disclaimers

The findings in this report are not to be construed as an official Department of the Army position unless so designated by other authorized documents.

Citation of manufacturer's or trade names does not constitute an official endorsement or approval of the use thereof.

Destroy this report when it is no longer needed. Do not return it to the originator.

Army Research Laboratory
Adelphi, MD 20783-1197

ARL-TR-5853 **December 2011**

Progress in Materials Synthesis and Processing of Barium Titanium Oxide ($BaTiO_3$) and Barium Strontium Titanium Oxide ($BaTiSrO_3$) Films for Uncooled Infrared (IR) Detector Applications

Wendy L. Sarney, Kimberley A. Olver, and John W. Little
Sensors and Electron Devices Directorate, ARL

Frank E. Livingston
The Aerospace Corporation

and

Krisztian Niesz and Daniel E. Morse
Institute for Collaborative Biotechnologies
University of California Santa Barbara

REPORT DOCUMENTATION PAGE

Form Approved
OMB No. 0704-0188

1. REPORT DATE *(DD-MM-YYYY)*	2. REPORT TYPE	3. DATES COVERED (From - To)
December 2011	Final	

4. TITLE AND SUBTITLE

Progress in Materials Synthesis and Processing of Barium Titanium Oxide ($BaTiO_3$) and Barium Strontium Titanium Oxide ($BaTiSrO_3$) Films for Uncooled Infrared (IR) Detector Applications

5a. CONTRACT NUMBER

5b. GRANT NUMBER

5c. PROGRAM ELEMENT NUMBER

6. AUTHOR(S)

Wendy L. Sarney, Kimberley A. Olver, John W. Little, Frank E. Livingston, Krisztian Niesz, and Daniel E. Morse

5d. PROJECT NUMBER

5e. TASK NUMBER

5f. WORK UNIT NUMBER

7. PERFORMING ORGANIZATION NAME(S) AND ADDRESS(ES)

U.S. Army Research Laboratory
ATTN: RDRL-SEE-I
2800 Powder Mill Road
Adelphi, MD 20783-1197

8. PERFORMING ORGANIZATION REPORT NUMBER

ARL-TR-5853

9. SPONSORING/MONITORING AGENCY NAME(S) AND ADDRESS(ES)

10. SPONSOR/MONITOR'S ACRONYM(S)

11. SPONSOR/MONITOR'S REPORT NUMBER(S)

12. DISTRIBUTION/AVAILABILITY STATEMENT

Approved for public release; distribution unlimited.

13. SUPPLEMENTARY NOTES

14. ABSTRACT

This report describes the highlights and summary of the year 2, quarter four (Y2Q4) progress for the 6.2 project "Improved Sensitivity Low-Cost Uncooled IR Detector Focal-Plane Arrays." This work occurred during the January 2010–May 2010 time period. The program goals for Y2Q4 corresponded to the continued expansion of our barium titanium oxide ($BaTiO_3$) nanomaterial synthesis capabilities and deposition methods; laser-induced pyroelectric phase conversion studies and nanoscale characterization of the pyroelectric activation process; and fabrication of infrared (IR) test heterostructures for pyroelectrical analysis, along with the development of a technique for generating the requisite IR absorbing layer.

15. SUBJECT TERMS

Uncooled infrared

16. SECURITY CLASSIFICATION OF:			17. LIMITATION OF ABSTRACT	18. NUMBER OF PAGES	19a. NAME OF RESPONSIBLE PERSON
a. REPORT	b. ABSTRACT	c. THIS PAGE			Wendy L. Sarney
Unclassified	Unclassified	Unclassified	UU	28	19b. TELEPHONE NUMBER (*Include area code*) (301) 394-5761

Standard Form 298 (Rev. 8/98)
Prescribed by ANSI Std. Z39.18

Contents

List of Figures

List of Tables

Acknowledgments

We acknowledge support by the Institute for Collaborative Biotechnologies through grant DAAD19-03-D-0004 from the U.S. Army Research Office and The Aerospace Corporation Independent Research and Development (IR&D) Program and the Product and Development Program (PDP).

1. Introduction

This report describes the highlights and summary of the year 2, quarter four (Y2Q4) progress for the 6.2 project "Improved Sensitivity Low-Cost Uncooled IR Detector Focal-Plane Arrays." This work occurred during the January 2010–May 2010 time period. The project schedule for year 2 is summarized in figure 1.

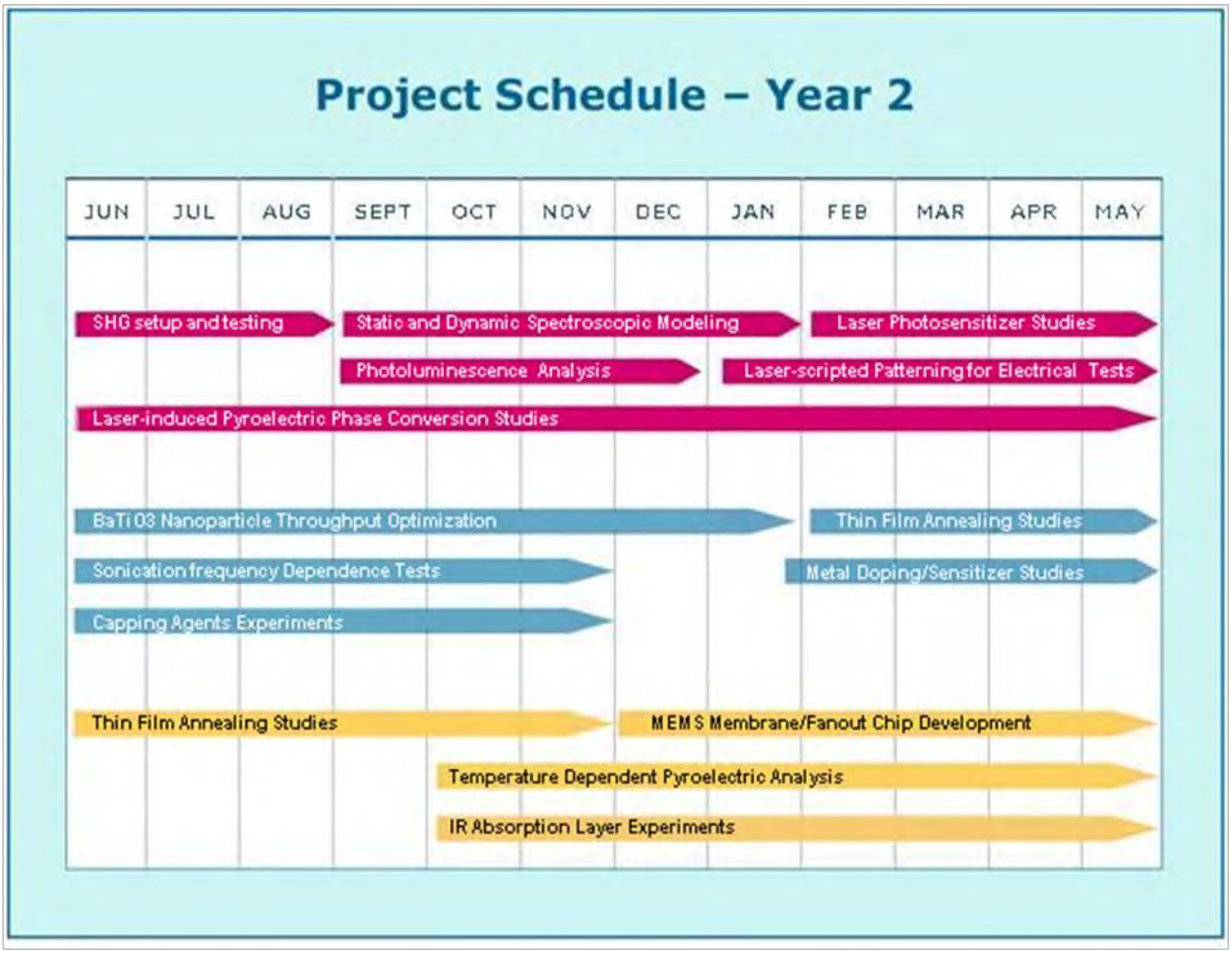

Figure 1. Project schedule.

The program goals for Y2Q4 corresponded to the continued expansion of our barium titanium oxide ($BaTiO_3$) nanomaterial synthesis capabilities and deposition methods; laser-induced pyroelectric phase conversion studies and nanoscale characterization of the pyroelectric activation process; and fabrication of infrared (IR) test heterostructures for pyroelectrical analysis, along with the development of a technique for generating the requisite IR absorbing layer. Respective team highlights include the following:

- *Aerospace:* This team conducted laser-scripted pixelation and pyroelectric activation of 8x8 pixel subarrays and 4x4-(8x8) pixel master arrays on Institute for Collaborative Biotechnologies (ICB) perovskite thin-film test structures for electrical characterization by the U.S. Army Research Laboratory (ARL). We successfully implemented piezoresponse force microscopy (PFM) techniques for the nanoscale ferroelectric analysis of the laser-induced pyroelectric phase activation process in perovskite thin films. Efforts also focused on the optical analysis and laser scripted processing of cerium (Ce)-doped perovskite nanoparticle thin films for enhanced laser-induced phase conversion efficiency.
- *ICB:* This team extended the bio-inspired vapor diffusion catalytic methods to include the synthesis, functionalization and deposition of perovskite nanoparticle ($BaTiO_3$, $Ba_{1-x}Sr_xTiO_3$) thin films comprising different compositions and thickness, along with the inclusion of Ce-dopant for enhanced ultraviolet (UV) absorption and improved laser-induced pyroelectric phase activation. Surface stabilization of the $BaTiO_3$ nanoparticles was also achieved using polyvinylpyrrolidone (PVP), which was found to facilitate the formation of stable colloids of $BaTiO_3$ and thereby mitigate the need for additional pre-deposition dispersion steps with carboxylic acids.
- *ARL:* This team continued with the development and refinement of the nanostructured IR absorbing layer, including optical absorption analysis of the nanostructures as a function of etch time. We established an electrical measurement system for frequency and temperature dependent capacitance/conductance measurements on native and laser-processed perovskite thin films, and fabricated 8x8 standard reference (titanium platinum [Ti/Pt]-silicon dioxide [SiO_2]) capacitor structures for baseline electrical testing. High resolution nanoscale characterization of re-dispersed barium strontium titanium oxide ($Ba_{1-x}Sr_xTiO_3$ or BSTO) nanoparticles was also accomplished.

All project teams have accomplished their respective planned milestones for Y2Q4. Highlights of the major activities are provided in sections 2 through 4.

2. Progress by the Aerospace Corporation (Aerospace)

2.1 Laser-scripted Direct-write Processing of $BaTiO_3$ and $BaSrTiO_3$ Thin Films for Electrical Analysis

2.1.1 CAD-CAM Patterning of Pixel Arrays

Our recent efforts in year 2 have focused on the digitally scripted laser genotype direct-write processing of ICB-provided $BaTiO_3$ and $BaSrTiO_3$ thin films, with particular emphasis on the systematic correlation of the laser processing parameters with the (pyro)electrical properties and IR responsiveness of the perovskite test structures. Based on the existing and preferred ARL mask geometries for metal contact deposition, our recent studies include laser processing

exposure patterns that comprise 8x8 pixel sub-arrays and 4x4-(8x8) pixel master arrays, as depicted in figures 2 and 3. Figure 2 shows a computer-assisted design (CAD) representation of a single 8x8 sub-array comprising 64 individual pixels, where the pixel dimensions are 100 μm x 100 μm with a lateral spacing of 100 μm and a center-to-center spacing of 200 μm. Each pixel is laser patterned using a sequential line fill with a lateral step-over that is comparable to the laser spot size (1–3 μm). Equivalent laser processing parameters—in the form of laser pulse "scripts" that are "linked" on a per spot basis to the tool path geometry in Cartesian space and contain specific information on laser pulse energy, polarization, wavelength, etc.—are applied to a series of four pixels so that 16 sets of laser processing parameters or "scripts" are administered to each 64 pixel set.

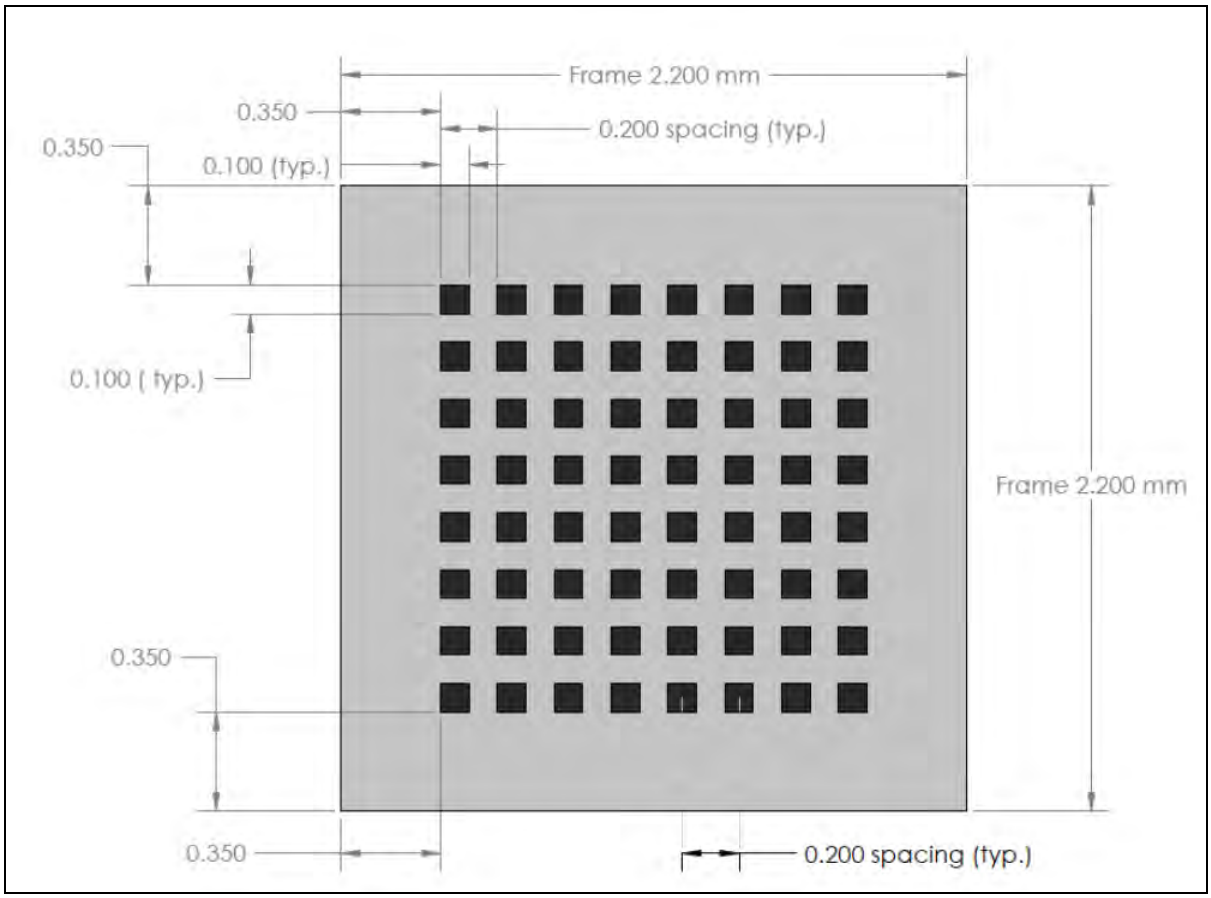

Figure 2. CAD illustration of a single 8x8 sub-array comprising 64 individual pixels, where the pixel dimensions are 100 μm x 100 μm with a center-to-center spacing of 200 μm. Each 8x8 pixel sub-array is enclosed in a 2.2 mm x 2.20 mm frame for visual reference and deposition mask alignment.

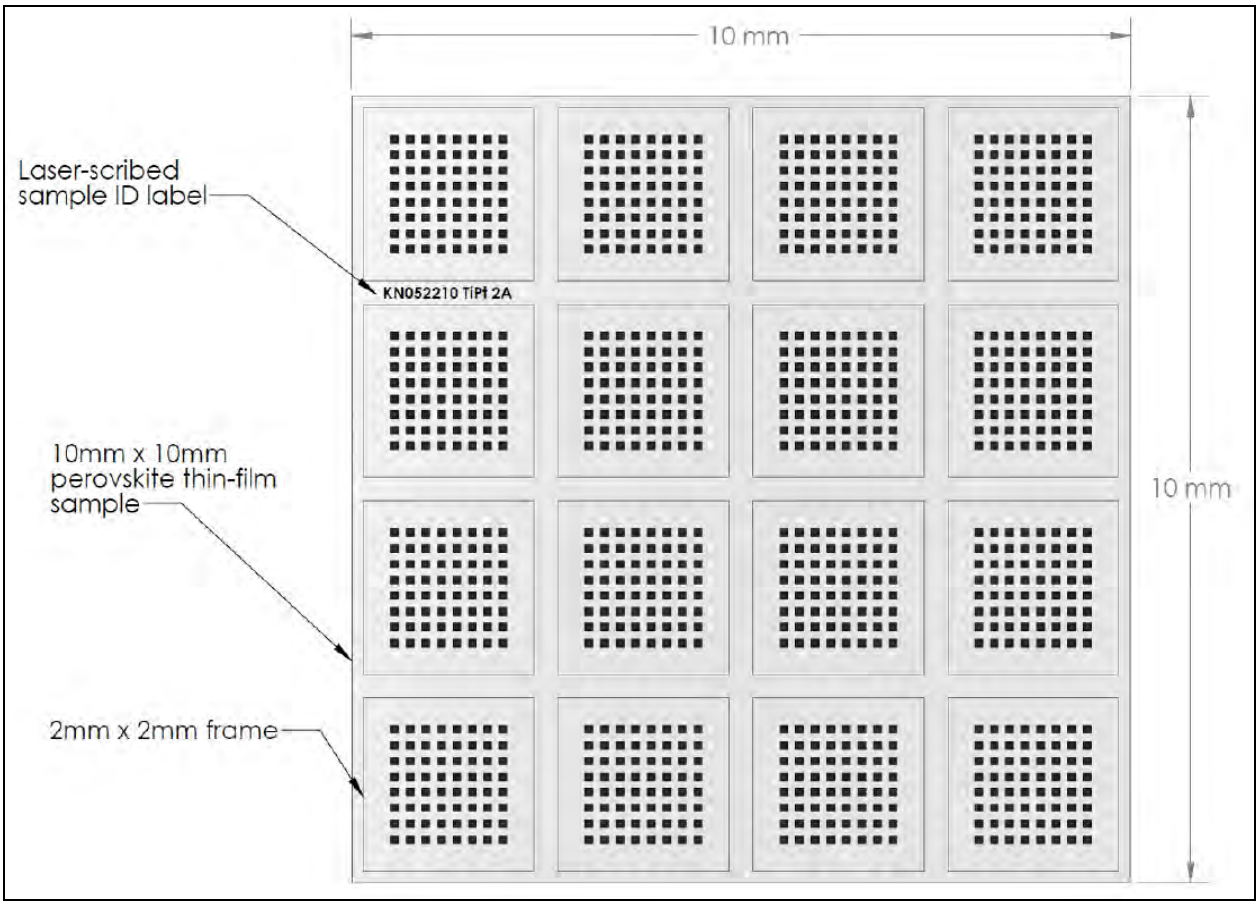

Figure 3. CAD illustration of a 4x4-(8x8) master array comprising 1024 pixels and sixteen 8x8 pixel sub-arrays.

Figure 3 displays a CAD illustration of a 4x4 master array of the 8x8 sub-arrays patterned on a standard 10 mm x 10 mm substrate, where the 16 8x8 pixel sub-arrays are processed using equivalent laser parameters and correspond to a total of 1024 laser-pixelated regions per sample. This laser-scripted redundancy can be implemented to assess the reproducibility of pyroelectric phase activation and film homogeneity across the entire spin-cast perovskite sample.

For visual reference and to facilitate the mask alignment procedure for metal contact deposition by ARL, each of the 16 8x8 pixel sub-arrays is enclosed by a 2.200 μm x 2.200 μm frame with a 100 m width. The frames are created using laser-controlled ablative patterning and the laser power is set to gently ablate or desorb the perovskite thin film without damage to the underlying Ti/Pt:silicon (Si) substrate. The distance from the outer edge of each of the four frame corners to the nearest corners of the four adjacent pixels (i.e., pixels 1, 8, 57, and 64) is 350 μm.

2.1.2 Laser-induced Pixelation/Pyroelectric Activation

Preliminary laser-scripted patterning and pixel array fabrication experiments were performed on organic polyimide thin films, such as Kapton™. These polymer-based films retain a very low thermal ablation threshold and are therefore useful in verifying high precision control of incident

photon flux and revealing the possible existence of excessive heat loading effects and residual thin-film damage. Additionally, low fluence laser exposure patterning of the organic thin films can be used to compare the laser-scripted pattern dimensions with the CAD-computer aided manufacturing (CAM) geometries and help elucidate any deviations or discrepancies.

Figures 4 and 5 show a series of low and high magnification photomicrographs of composite 4x4-(8x8) pixel arrays and 8x8 pixel sub-arrays that were laser patterned on a Kapton thin film. The 1024 individual pixel elements, along with the sub-array frames and sample identification label, were fabricated using laser irradiation at λ=355 nm, a pulse repetition rate of 80 MHz, and a pulse duration of 10 ps. The per-pulse fluence employed for pixelation and frame/ID were E=0.88 mJ·cm^{-2} and E=2.00 mJ·cm^{-2}, respectively. A non-contact white light optical profilometer was used to measure the laser-fabricated pixels, lateral pixel spacing distances, and frame dimensions. The standard deviation between the laser-scripted pattern dimensions and the user-defined CAD geometries was measured to be less than 0.05% and is consistent with the nominal resolution and repeatability of the XYZ air bearing translation stage encoders of 40 nm.

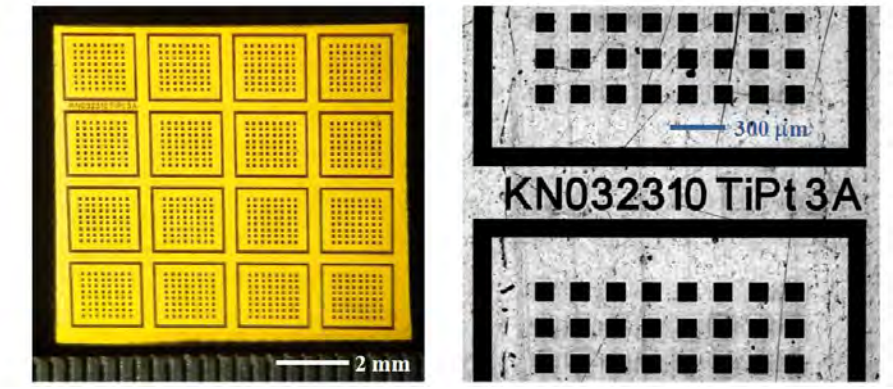

Figure 4. Low (left) and high (right) magnification photomicrographs acquired following the laserscripted pixelation of 4x4-(8x8) arrays on a Kapton film on quartz at λ = 355 nm.

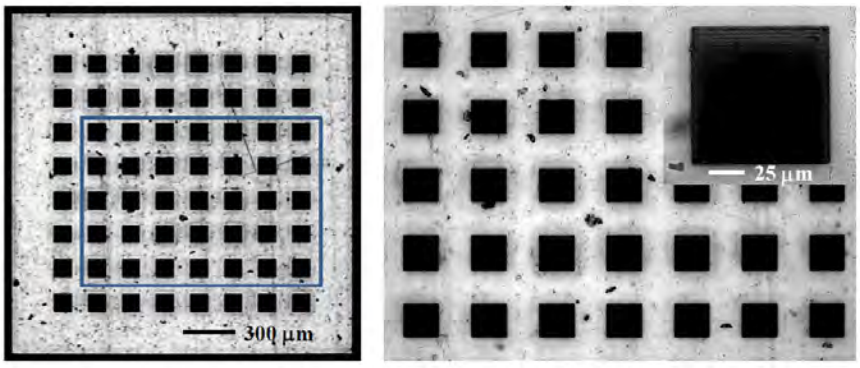

Figure 5. Low (left) and high (right) magnification photomicrographs of an individual 8x8 pixel array acquired following the laser-scripted patterning of a Kapton film at λ = 355 nm. The inset (upper right) shows a single 100 µm x 100 µm pixel element.

During the fourth quarter, digitally scripted laser genotype processing techniques were also implemented to create patterned and pyroelectrically active pixel arrays on ICB undoped and CeO_2-doped $BaTiO_3$ and $Ba_{1-x}Sr_xTiO_3$ thin films deposited on Ti/Pt:Si substrates. Laser-scripted direct-write laser pulse modulation was used to convert pixelated regions (100 μm x 100 μm) of the perovskite thin-films from the pyroelectrically inactive cubic polymorph to the pyroelectrically active tetragonal polymorph. Figure 6 shows several photomicrographs of an undoped $BaTiO_3$ thin film sample following laser pixelation and pyroelectric phase activation at λ = 355 nm (80 MHz, 10 ps full width at half maximum [FWHM]). The $BaTiO_3$:Ti/Pt:Si sample was 10 mm x 10 mm in size, and contained sixteen 8x8 pixel sub-arrays for a total of 1024 laser-pixelated regions. The pixelated regions were patterned using 16 sets of laser processing parameters—i.e., genotype laser pulse "scripts"—for each 8x8 pixel sub-array. The large laser processing parameter set will help to optimize the pyroelectric phase activation protocol and facilitate the correlation of the laser processing conditions with the electrical properties of the pixel domains. The variation in pixel contrast uniformity and darkness arise from the diverse set of laser processing pulse scripts that were implemented for patterning, and do not correspond to inhomogeneities or variegations in the perovskite thin film.

A set of laser-pixelated $BaTiO_3$:Ti/Pt:Si and $BaTiO_3$-CeO_2:Ti/Pt:Si samples have been shipped to ARL, and electrical analysis and pyroelectrical responsiveness tests are now underway.

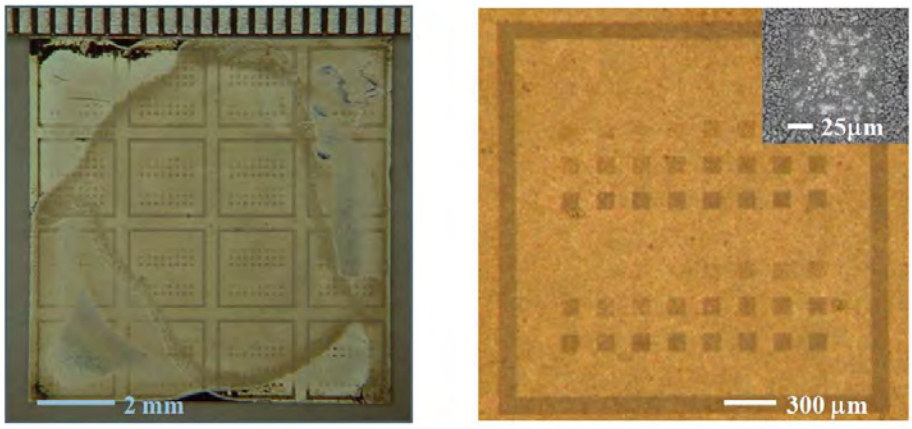

Figure 6. Low (left) and high (right) magnification photomicrographs acquired following the laser scripted pixelation and pyroelectric activation of 4x4-(8x8) arrays on a pure, undoped $BaTiO_3$ thin-film at λ = 355 nm. The inset (upper right) shows a single 100 μm x 100 μm pixel element.

2.2 Nanoscale Ferroelectric Characterization of Laser-induced Pyroelectric Activation in ICB Perovskite Thin Films

Our fourth quarter efforts for year 2 have also focused on the nanoscale characterization of the ferroelectric properties of laser-processed barium titanate thin films. We are continuing to develop the use of scanning PFM techniques for nanoscale analysis of the laser-induced $BaTiO_3$ cubic-to-tetragonal pyroelectric phase transformation, along with an assessment of the relative

magnitudes of the ferroelectric phase contrasts of the respective nonferroelectric (nFE)/ ferroelectric (FE) domains. As noted in our prior quarterly reports, PFM permits direct imaging of ferroelectric domain structures with nanometer-scale resolution (~3–10 nm) and is ideally suited for post-laser-processing examination of the perovskite thin films due to its relative insensitivity to topography and ease of implementation. We have successfully augmented and tailored our traditional atomic force microscopy (AFM) instrument for PFM operation, where the mechanical response of the sample is measured during local electrical excitation by the AFM probe tip. A modulated AC voltage is applied between the underlying Ti/Pt:Si substrate and conductive AFM/PFM tip during contact mode scanning. Using lock-in amplifier techniques, the local electromechanical displacement can be decoupled from the topographical displacement via the phase shift between the rapidly oscillating ac field and the slow cantilever displacement feedback (figure 7). The static cantilever deflection corresponds to the surface profile variations and topography, while the modulated cantilever oscillations are related to the piezoresponse of the perovskite sample.

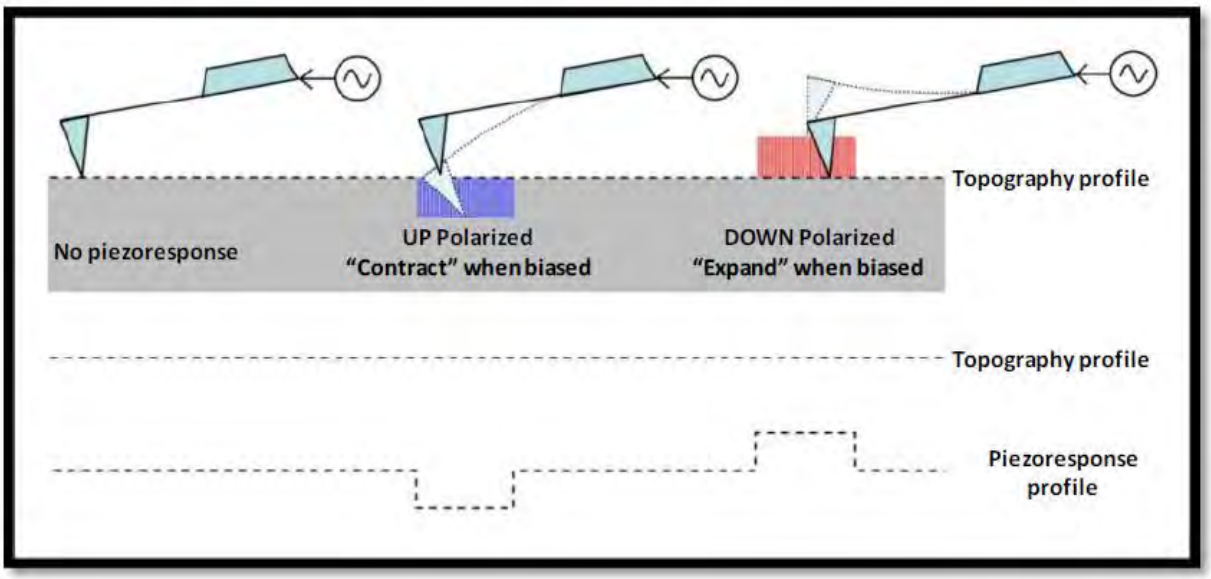

Figure 7. PFM concept where the mechanical response of the thin film is measured during local high frequency excitation by the AFM probe tip. The topography and piezoresponse profiles can be simultaneously acquired and decoupled to provide surface roughness and ferroelectric phase contrast information.

Figure 8a displays a PFM image of a $BaTiO_3$ thin-film sample that was acquired prior to laser-scripted exposure at $\lambda = 355$ nm and shows no in-plane (polarization parallel to sample surface) ferroelectric phase contrast for the as-received cubic crystalline $BaTiO_3$ thin film. Following laser-scripted exposure at =355 nm (~$1x10^6$ pulses, per-pulse fluence = 2.5 $mJ \cdot cm^{-2}$), the PFM results in figure 8b reveal appreciable ferroelectric phase contrast and confirm successful pyroelectric conversion to the tetragonal phase. Figures 9a and 9b show similar PFM contrast behavior for the unexposed and laser-processed $BaTiO_3$ thin film, where the measured

piezoresponse signals correspond to polarization dipoles that are aligned perpendicular to the sample surface. The laser-structured and pyroelectrically activated regions appear uniform and retain ferroelectric domain sizes of ~50–500 nm.

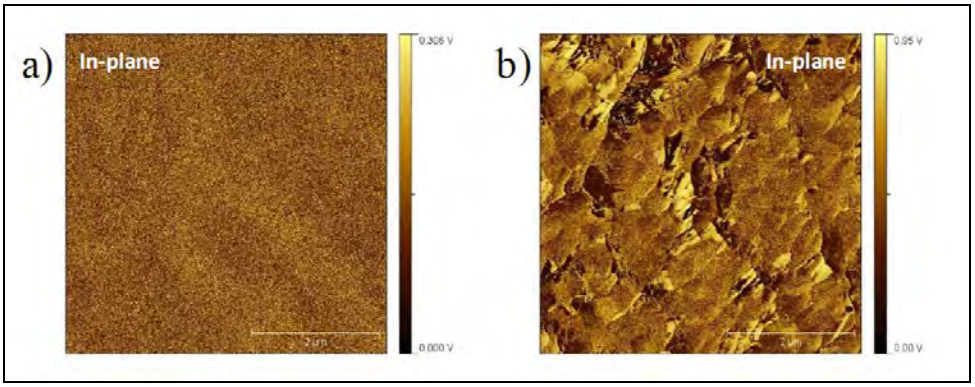

Figure 8. PFM images (in-plane polarization) of $BaTiO_3$ thin films that were acquired (a) prior to laser exposure and (b) following laser-scripted patterning and pyroelectric phase conversion at λ = 355 nm. The image sizes are 5 μm x 5 μm.

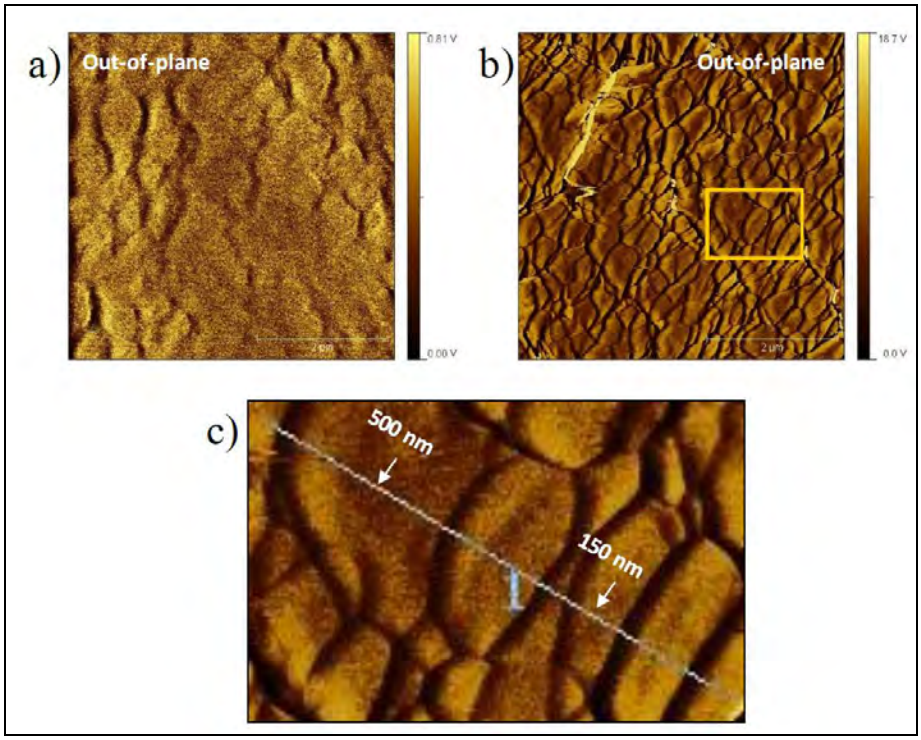

Figure 9. PFM images (out-of-plane polarization) of $BaTiO_3$ thin films that were acquired (a) prior to laser exposure and (b) following laser-scripted patterning and pyroelectric phase conversion at λ = 355 nm. The image sizes are 5 μm x 5 μm. (c) High magnification PFM image showing typical ferroelectric domain sizes of 50–500 nm.

2.3 Measurement of Optical Band Gap Energies for CeO_2-doped Perovskite Thin Films

Expanding upon our prior detailed studies concerning the influence of perovskite film thickness on the intrinsic optical bandgap energies of the nanostructured films, we are now examining the optical properties of *doped* perovskite nanoparticle thin films. The intent is to incorporate the appropriate photo-active constituents (e.g., CeO_2) into the perovskite nanoparticles to enhance the UV absorption in the native thin films and thereby improve the laser-induced pyroelectric phase conversion efficiency and reduce the incident laser energy required for pyroelectric activation. The prudent selection of dopant type and concentration will also facilitate the fine-tuning of the electrical properties of the perovskite thin films and may enable a broader range of pyroelectric responsiveness.

Our prior optical transmission studies indicated that for the thicker micron-sized $BaTiO_3$ films (>1 μm), inter-band transitions occur at wavelengths of λ<450–500 nm, and the transmission falls rapidly to less than 10% at wavelengths of λ<400 nm. In contrast, inter-band transitions occur at wavelengths of λ<300 nm for the thinner 200–500 nm-thick films, and the 10% cut-off occurs at UV wavelengths of <260 nm. Consequently, the absolute bandgap energies for the thinner and functionalized $BaTiO_3$ films are significantly *blue-shifted* compared with the thicker micrometer scale films. The calculated bandgap energies displayed the following trend with film thicknesses denoted in parentheses: E=3.27±0.4 eV (3–5 μm), 3.84±0.2 eV (0.5–1 μm), 3.95±0.1 eV (300–500 nm), and 4.12±0.05 eV (200–300 nm). The film-thickness dependent behavior of the bandgap energy severely impacts the selection of the appropriate laser processing wavelengths and other laser parameters that are requisites for efficient laser energy-material coupling and optimal pyroelectric phase conversion. For low-cost rapid prototype manufacture of the IR sensor components, the use of a readily available commercial solid-state laser system is preferred.

Accordingly, and with our ICB collaborators, we have explored the effect of incorporating CeO_2 into the perovskite nanoparticles during synthesis as a means to *red-shift* the absorption band edge of the nanostructured films, thereby lowering the optical bandgap energies and reducing the total incident laser irradiation required for complete pyroelectric phase transformation. Figure 9 shows the optical transmission spectra that were measured for pure $BaTiO_3$ and CeO_2-doped (0.03 wt%) $BaTiO_3$ thin films. The $BaTiO_3$ samples correspond to 1-layer spin coatings with a nominal film thickness of ~550 nm. The optical results presented in figure 10 are encouraging, and reveal that low impurity doping with CeO_2 can be used to reduce the UV transmission for <350 nm and induce a red-shift in the band gap energy. For example, the bandgap energy and 10% T cut-off wavelength for the pure undoped 550-nm-thick $BaTiO_3$ films were measured to be E=4.02±0.05 eV and =264.5 nm, respectively. However, the bandgap energy has been reduced to E=3.87±0.05 eV and the 10% T cut-off has been shifted to a longer wavelength of λ = 300 nm for the CeO_2- doped $BaTiO_3$ film of comparable thickness. The optical results for the pure and CeO_2-doped $BaTiO_3$ and $BaSrTiO_3$ films are summarized in table 1.

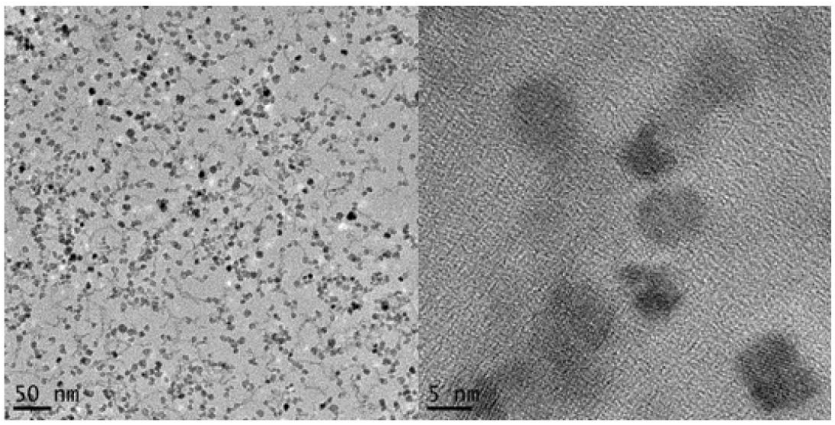

Figure 10. Optical transmission spectra measured for pure and CeO_2-doped $BaTiO_3$ and $BaSrTiO_3$ films with thicknesses of 550 nm. The inset shows the cerium (Ce^{4+}) absorption spectrum.

Table 1. Summary of the optical results for the pure and CeO_2-doped $BaTiO_3$ and $BaSrTiO_3$ films.

Number of Spin Coat Layers	Film Thickness (nm)	Band Gap Energy (eV)/10% T Cut-off (nm)							
		$BaTiO_3$		$BaTiO_3$-CeO_2		$BaSrTiO_3$		$BaSrTiO_3$-CeO_2	
1	550	4.02	264.5	3.87	300.0	3.85	298.0	3.70	318.5
2	1100	3.91	280.0	3.78	315.0	----		----	
3	1440	3.80	296.5	3.73	323.5	----		----	

The inset in figure 10 shows the absorption spectrum that is associated with the Ce chromophore, and was derived from the difference between the CeO_2-doped and undoped perovskite thin-film. The primary spectral feature is an absorption peak located near =230–235 nm and corresponds to the Ce^{4+} oxidation state of Ce. A broad featureless absorption is also observed and extends beyond 250 nm. There is a rapid absorption fall-off for wavelengths >300 nm, and this behavior is likely responsible for the negligible change in absorption characteristics for the thicker (>1 μm) CeO_2-doped $BaSrTiO_3$ films.

3. Progress by the Institute for Collaborative Biotechnologies (ICB)

3.1 $BaTiO_3$ and $BaSrTiO_3$ Sample Preparation with Varying Compositions and Thickness; Surface Stabilization Studies with PVP

The ICB efforts focused on three critical areas regarding perovskite sample synthesis and thin-film preparation:

- Based on our previous experiences, samples with different compositions ($BaTiO_3$, $Ba_{1-x}Sr_xTiO_3$), with and without using additional Ce dopant were synthesized, functionalized with oleic acid and deposited from colloidal suspensions onto different types of substrates (quartz, Pt/Ti:Si). The depositions were carried out by layer-by-layer spinning using different numbers of deposition/annealing cycles to vary the perovskite film thickness. The samples were then sent to our collaborating partners at Aerospace and ARL for further investigations.
- Comprehensive sets of pure (undoped) and CeO_2-doped (0.03 wt%) $BaTiO_3$ and $Ba_{1-x}Sr_xTiO_3$ thin films were prepared and sent to Aerospace for laser-scripted processing and pixelation/activation studies, as well as optical analysis. These samples included systematic variation of the film thickness from 550 nm (1-layer spin coat) to 1440 nm (3-layer spin coat). $BaTiO_3$ and $Ba_{1-x}Sr_xTiO_3$ samples—in their nascent nanoparticle form—were synthesized and sent to ARL for thin-film test structure fabrication and electrical characterization.
- Experiments were conducted using PVP as surface stabilizing agent to form BaTi nanoparticles as stable colloids. Performing the synthesis this way the additional stabilizing step with oleic acid before depositions could be avoided. Adding PVP to the BaTi double alkoxide molecules dissolved in butanol (2:1 molar ratio of PVP-monolayer to BaTi-precipitate) indeed resulted in the formation of $BaTiO_3$ nanocrystals stable against aggregation (see figure 10).

4. Progress by ARL

4.1 Nanostructured IR Absorbing Layer Development

As explained in the prior quarter's report, thermal detectors require a layer similar to a thin coating of black paint that absorbs a wide range of wavelengths and heats up. The heat is transferred to the BT layer and the pyroelectric voltage is generated. We are developing a low-cost technique that is temperature-compatible with the bio-inspired $BaTiO_3$ films and with readout integrated circuit (ROIC) technology. The details of the process were given in the

previous quarterly report, but the main features of the technique involve forming nanoparticles of metal (e.g., gold [Au]) on an evaporated Si film and subsequently etching the Si with a dry etch. The Au particles mask the surface resulting in nanopilars of Si that have been shown to trap and absorb light strongly. We formed the particles on a Si wafer by heating a 5-nm evaporated Au film to 350 °C and etched pieces in a carbon tetrafluoride (CF_4) plasma for various times.

Figure 11 shows the absorption (relative to a bare Si wafer) at different wavelengths as a function of the etch time. Note that for this first set of samples, the highest absorption was obtained for a 20 s and was peaked at 1.5 μm wavelength. This wavelength is ideal for enhancing the near IR photoresponse of solar cells, and we are transitioning this technology to our quantum dot solar cell program.

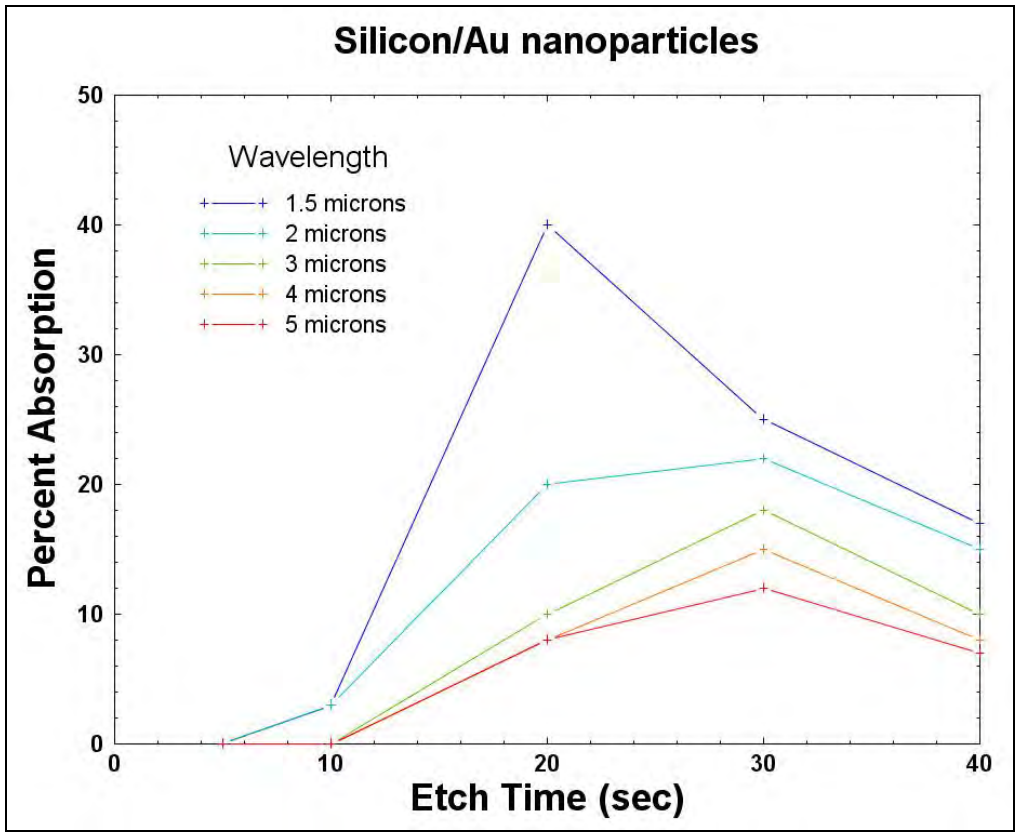

Figure 11. The absorption (relative to a bare Si wafer) at different wavelengths as a function of the etch time for the currently-developed IR absorption layer.

We are modifying the nanostructure to push the wavelength into the thermal imaging part of the spectrum (3–12 μm) and maximize the absorption strength. A new set of samples is being prepared with larger scale and deeper nanostructures and the results will be given in a subsequent report.

4.2 Frequency and Temperature Dependent Capacitance/Conductance Measurements

We have begun establishing a measurement system that will characterize the temperature and frequency dependence of the capacitance/conductance of the $BaTiO_3$ films (in order to determine the pyroelectric properties of the films). A Hewlett Packard 4280A precision fixed frequency (1 MHz) capacitance meter and a variable frequency (1 Hz–1 MHz) function generator/quadrature lock-in amplifier is used to measure the capacitance/conductance of our test samples. The system has been calibrated with a precision capacitance bridge. A variable temperature sample mount will be added soon.

Figures 12 and 13 show an 8 x 8 array (one column is for ground plane contact) of Ti/Pt–SiO_2 capacitors (100 x 100 microns) that we fabricated as a standard reference for the measurement system (this test structure has a known capacitance). These samples have the same configuration as the laser-modified BT films.

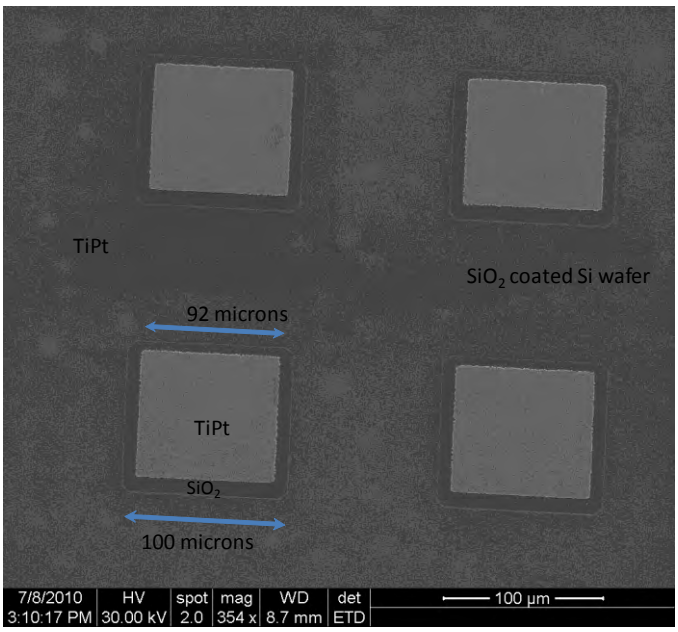

Figure 12. Transmission electron microscope (TEM) images of as-prepared BaTi nanoparticles stabilized with PVP.

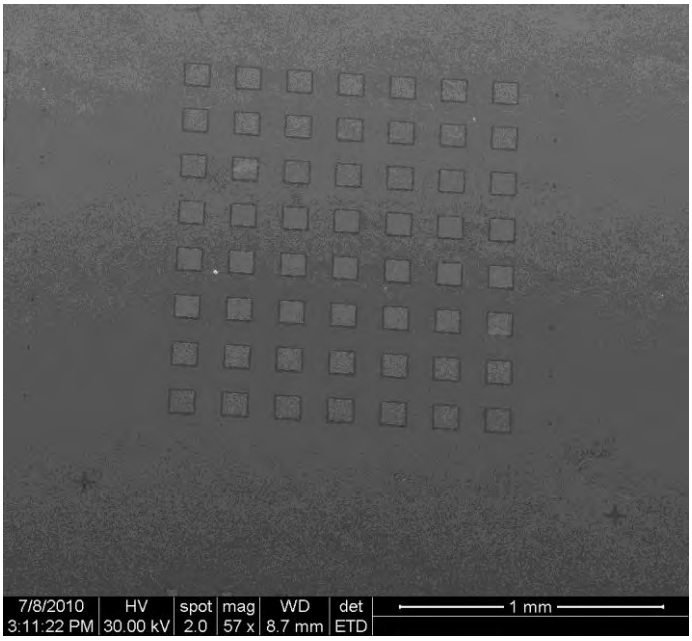

Figure 13. Capacitance test structure.

4.3 Nanoscale Characterization of BSTO Particles

In this quarter, the ICB sent vials of BSTO nanoparticles to ARL. As detailed in the prior report, BSTO has several desirable properties for both IR detector and laser processing applications. These include a relatively large dielectric constant, good pyroelectric response near room temperature, low dielectric loss and leakage current, and phase transition temperature controllable by the amount of strontium (Sr) incorporated.

The nanoparticles were capped with oleic acid, and then were precipitated and dried. At ARL, we re-dispersed the nanoparticles into isopropanol to prepare TEM grids.

Figure 14 is a TEM image of the barium strontium titanate (BST) powder (KN238). As with the previously examined $BaTiO_3$ nanoparticles, the TEM images show high-quality, single-crystalline nanoparticles. The particles in this particular vial measured around 6–7 nm.

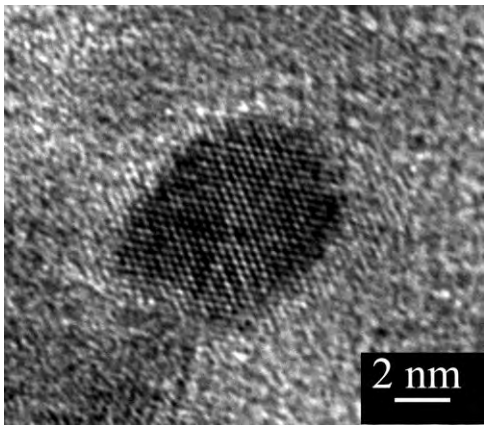

Figure 14. SEM image of an 8x8 array (one column is for ground plane contact) of 100 x 100 μm Ti/Pt-SiO_2 capacitors.

5. Plans and Goals for Year 3, Quarter 1

In the coming quarter, we will continue to expand our nanomaterial synthesis capabilities, laser processing techniques and pyroelectric phase conversion studies, and perovskite thin-film electrical characterization efforts:

- *ICB:* This team will finalize construction of the large-scale reactor and pursue trials of continuous-flow production with automated control, further investigate the in situ stabilization of $BaTiO_3$ nanoparticles using PVP, and continue to provide pure and doped $BaTiO_3$ and $Ba_{1-x}Sr_xTiO_3$ nanoparticle thin films to Aerospace and ARL for laser-scripted pixelation/pyroelectric activation studies and electrical characterization of thin-film test structures.
- *Aerospace:* This team will continue fabrication of laser-pixelated perovskite thin-film array test structures for electrical analysis and IR responsiveness measurements by ARL; measure local PFM hysteresis curves for unexposed and laser-processed perovskite thin films to extract piezoelectric constants and assess uniformity of phase conversion and intrinsic/residual stresses in the IR test structures; and explore the laser scripted processing of the IR absorbing overlayer to induce patterned pyroelectric phase conversion of the underlying perovskite thin film.
- *ARL:* This team will modify the IR nanostructures that comprise the absorbing layer to shift absorption into the thermal imaging region (3–12 μm) and optimize the absorption strength and integrate variable temperature sample mount into electrical measurement system for frequency and temperature dependent capacitance/conductance studies on native and laser-activated $BaTiO_3$ and $Ba_{1-x}Sr_xTiO_3$ thin-film test structures.

6. Metrics for Year 2 Quarter 4

6.1 Publications

1. Niesz, K.; Morse, D. E. Sonication-accelerated Catalytic Synthesis of Oxide Nanoparticles. *Nano Today* **2010**, *5*, 99–105.

6.2 Conferences and Symposia

1. Livingston, F. E.; Sarney, W. L.; Niesz, K.; Morse, D. E. Laser Direct-write Activation of Perovskite Nanoparticle Films for Thermal Detector Applications. Presented Poster at the *National Defense Industrial Association (NDIA) – 11th Annual Science & Engineering Technology Conference/DoD Tech. Exposition*, Charleston, SC, Apr. 12–15, 2010.

2. Niesz, K.; Reji, C.; Vargas, R. C.; Neilson, J.; Ould Ely, T.; Livingston, F. E.; Sarney, W. L.; Morse, D. E. Fabrication of Simple and Complex Oxide Nanoparticles by Sonication Assisted Vapor Diffusion Catalysis: Synthesis, Characterization and Applications. Presented poster at the *239th ACS National Meeting and Exposition*, San Francisco, Mar. 21, 2010.

3. Livingston, F. E.; Sarney, W. L.; Niesz, K.; Little, J. W.; Olver, K. A.; Morse, D. E. Laser Tailoring of Bio-inspired Thin-films for Improved Sensitivity, Low-cost Uncooled IR Detector FPAs. Presented poster at the *2010 Institute for Collaborative Biotechnologies (ICB) Army-Industry Collaboration Conference*, UC Santa Barbara, CA, Mar. 3–4, 2010.

List of Symbols, Abbreviations, and Acronyms

AFM	atomic force microscopy
ARL	U.S. Army Research Laboratory
Au	gold
$BaTiO_3$	barium titanium oxide
BST	barium strontium titanate
BSTO	barium strontium titanium oxide
CAD	computer-assisted design
CAM	computer aided manufacturing
Ce	cerium
CF_4	carbon tetrafluoride
FE	ferroelectric
FWHM	full width at half maximum
ICB	Institute for Collaborative Biotechnologies
IR	infrared
IR&D	Independent Research and Development
nFE	nonferroelectric
PDP	Product and Development Program
PFM	piezoelectric force microscopy
PVP	polyvinylpyrrolidone
ROIC	readout integrated circuit
Si	silicon
SiO_2	silicon dioxide
Sr	strontium
TEM	transmission electron microscope

Ti/Pt	titanium platinum
UV	ultraviolet
Y2Q4	year two, quarter four

NO. OF COPIES	ORGANIZATION
1 ELEC	ADMNSTR DEFNS TECHL INFO CTR ATTN DTIC OCP 8725 JOHN J KINGMAN RD STE 0944 FT BELVOIR VA 22060-6218
1 CD	OFC OF THE SECY OF DEFNS ATTN ODDRE (R&AT) THE PENTAGON WASHINGTON DC 20301-3080
1	US ARMY RSRCH DEV AND ENGRG CMND ARMAMENT RSRCH DEV & ENGRG CTR ARMAMENT ENGRG & TECHNLGY CTR ATTN AMSRD AAR AEF T J MATTS BLDG 305 ABERDEEN PROVING GROUND MD 21005-5001
1	US ARMY INFO SYS ENGRG CMND ATTN AMSEL IE TD A RIVERA FT HUACHUCA AZ 85613-5300
1	COMMANDER US ARMY RDECOM ATTN AMSRD AMR W C MCCORKLE 5400 FOWLER RD REDSTONE ARSENAL AL 35898-5000
1	US GOVERNMENT PRINT OFF DEPOSITORY RECEIVING SECTION ATTN MAIL STOP IDAD J TATE 732 NORTH CAPITOL ST NW WASHINGTON DC 20402
2	INSTITUTE FOR COLLABORATIVE BIOTECHNOLOGIES UNIVERSITY OF CALIFORNIA, SANTA BARBARA ATTN D MORSE ATTN K NIESZ SANTA BARBARA CA 93106-5100
1	THE AEROSPACE CORPORATION MICRO/NANOTECHNOLOGY DEPARTMENT SPACE MATERIALS LABORATORY ATTN F LIVINGSTON 2350 E EL SEGUNDO BLVD EL SEGUNDO CA 90245

NO. OF COPIES	ORGANIZATION
6	US ARMY RSRCH LAB ATTN IMNE ALC HRR MAIL & RECORDS MGMT ATTN RDRL CIO LL TECHL LIB ATTN RDRL CIO MT TECHL PUB ATTN RDRL SEE I J LITTLE ATTN RDRL SEE I K OLVER ATTN RDRL SEE I W SARNEY ADELPHI MD 20783-1197

TOTAL: 15 (1 ELEC, 1 CD, 13 HCS)

INTENTIONALLY LEFT BLANK.